Thiol-ethylene bridged PMO : a high capacity regenerable mercury adsorbent via intrapore mercury thiolate crystal formation

Thiol-ethylene bridged PMO: a high capacity regenerable mercury adsorbent via intrapore mercury thiolate crystal formation

Dolores Esquivel,[a,b*] Judith Ouwehand,[a] Maria Meledina,[c] Stuart Turner,[c] Gustaaf Van Tendeloo,[c] Francisco J. Romero-Salguero,[b] Jeriffa De Clercq[d] and Pascal Van Der Voort[a *]

[a] *Department of Inorganic and Physical Chemistry, Center for Ordered Materials, Organometallics & Catalysis, Ghent University, Krijgslaan 281-S3, 9000 Ghent, Belgium.*

[b] *Departamento de Química Orgánica, Instituto Universitario de Investigación en Química Fina y Nanoquímica IUIQFN, Facultad de Ciencias, Universidad de Córdoba, Campus de Rabanales, Edificio Marie Curie, E-14071 Córdoba, España*

[c] *Electron Microscopy for Materials Science (EMAT), University of Antwerp, Groenenborgerlaan 171, 2020 Antwerp, Belgium.*

[d] *Industrial Catalysis and Adsorption Technology (INCAT), Department of Chemical Engineering and Technical Chemistry, Faculty of Engineering and Architecture, Ghent University, Valentin Vaerwyckweg 1, 9000 Ghent, Belgium.*

**corresponding authors; q12esmem@uco.es* (Dolores Esquivel), *pascal.vandervoort@ugent.be* (Pascal Van Der Voort).

Graphical abstract

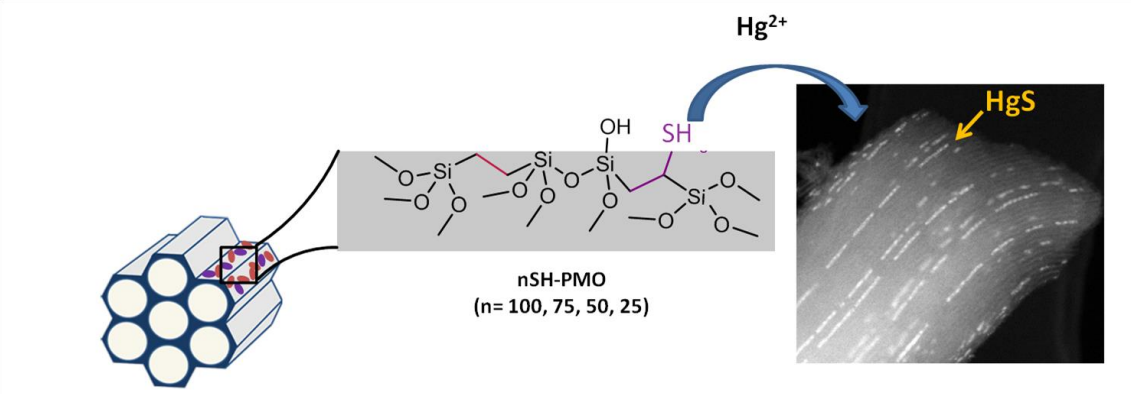

HIGHLIGHTS

- Thiol-ethylene bridged PMOs with controllable thiol loading were synthesized.
- SH-PMO adsorbed up to 1183 mg/g Hg^{2+} from aqueous solution
- SH-PMO adsorbents were regenerated and reused several times.
- Formation of mercurythiolate nanocrystals in the pores after Hg^{2+} uptake.

Abstract

Highly ordered thiol-ethylene bridged Periodic Mesoporous Organosilicas were synthesized directly from a homemade thiol-functionalized bis-silane precursor. These high surface area materials contain up to 4.3 mmol/g sulfur functions in the walls and can adsorb up to 1183 mg/g mercury ions. Raman spectroscopy reveals the existence of thiol and disulfide moieties. These groups have been evaluated by a combination of Raman spectroscopy, Ellman's reagent and elemental analysis. The adsorption of mercury ions was evidenced by different techniques, including Raman, XPS and

porosimetry, which indicate that thiol groups are highly accessible to mercury. Scanning transmission electron microscopy combined with EDX showed an even homogenous distribution of the sulfur atoms throughout the structure, and have revealed for the first time that a fraction of the adsorbed mercury is forming thiolate nanocrystals in the pores. The adsorbent is highly selective for mercury and can be regenerated and reused multiple times, maintaining its structure and functionalities and showing only a marginal loss of adsorption capacity after several runs.

Keywords: periodic mesoporous organosilicas; thiol-functionality; Hg-adsorption; mercury thiolate nanocrystals; regeneration

1. Introduction

Mercury, classified by the United States Environmental Protection Agency and European Union as a priority hazardous substance, is a relevant environmental issue.[1, 2] Among the different methods reported to remove mercury from (waste)water,[3-6] adsorption has been found to be a very promising method because of its efficiency and its selectivity. Mercury, as a soft Lewis acid (HSAB theory – Pearson 1963),[7] reacts more rapidly and forms stronger bonds with “soft” functional ligands containing sulfur or nitrogen atoms. Therefore, adsorbents with a large surface area, large (ordered) porosity and high loading of S-containing chelating groups are ideal candidates for effective and selective removal of mercury ions from wastewater.

Thiol-functionalized mesoporous silica materials with high surface areas and ordered mesoporous structures have been widely employed as effective and recyclable

adsorbents for the removal of heavy metal ions from aqueous solutions.[8-13] The thiol ligands are introduced into the silica framework, either by grafting of organotrialkoxysilanes ($HS-(CH_2)_nSi(OR`)_3$) onto the surface of the mesoporous silicas or by co-condensation of such organotrialkoxysilanes with tetraalkoxysilanes ($Si(OR`)_4$) in the presence of the structure-directing agent. Both methods are limited by relatively low loadings of the S-containing chelating groups, inhomogeneity of the active species and the possibility of pore blocking (grafting) or loss of mesoscopic structure (co-condensation). Also, the hydrolytic stability of the grafted silane species is relatively weak.[14]

In 1999, several research groups described simultaneously the invention of the Periodic Mesoporous Organosilica (PMO).[15-17] This class of hybrid materials is synthesized from bridged organosilanes of the type $(R'O)_3Si-R-Si(OR')_3$, where R' is a methyl or ethyl group and R designates the functional organic bridge. The same soft templating approach used for the synthesis of ordered mesoporous silicas is applied to form these materials. PMO materials have a homogeneous distribution of functional groups and do not suffer from pore blocking, as the active groups are embedded in the walls of the material. They have a very high mechanical, hydrothermal and hydrolytic stability.[18, 19] An important limitation is however the need to have a relatively small and rigid organic bridging group, R, to ensure the formation of a periodic mesoporous structure and the permanent porosity of the material after removal of the soft template. Several reviews have appeared on the types and functionalities of these organic bridges in PMOs and their applications.[14, 18, 20, 21] Although numerous functionalities have been incorporated as bridging moieties, mainly PMOs containing isocyanurate [22-24] and thioether (-S-S- or -S-S-S-S-)[25-28] groups have shown high adsorption affinity for heavy metals ions. As both functional precursors are too large and too flexible to

assemble directly a rigid PMO framework, a co-condensation procedure with a pure silica source, TEOS, was required.

Alternatively, the organic bridges in the PMOs can be post-functionalized with thiol groups. We reported that ethenylene bridged PMOs functionalized with thiolpropyl groups by Grignard chemistry are very selective and stable adsorbents in "Diffusive Gradient Thin Film (DGT)" probes.[29, 30] In an alternative strategy, a vulcanization procedure to introduce sulfur moieties in an ethenylene bridged PMO has been published to obtain a very stable adsorbent.[31]

Until now, the common methods of making thiol-functionalized periodic mesoporous organosilica materials involve grafting or co-condensation processes of a bis-silane precursor and a mercaptopropyltrialkoxysilane (MPTES or MPTMS), because of the non-availability of such functionality on bridged silsesquioxane precursors.[29, 32-34] This aspect has recently changed due to the development of novel bis-silane precursors containing thiol-ethylene[35] or thiophenol[36] as bridging organic functions.

In this context, our recently developed thiol-bissilane precursor provides an approach to synthesize a new thiol-ethylene bridged PMO material.[35] In this precursor, synthesized by thiol acid-ene click chemistry, every ethylene bridging group holds one thiol group. Upon condensation into a templated porous material, the resulting PMO has an unprecedented high sulfur loading, up to 4.3 mmol/g. In contrast to the above-mentioned approaches, this small and rigid thiol-functional silsesquioxane precursor is able to self-assemble into well-ordered mesostructures which avoids co-condensation/grafting or post-functionalization processes to incorporate such functionality. Likely, the homogenous distribution of the -SH functional groups within

the porous PMO framework leads to a unique adsorbent material where active sites are completely accessible for Hg^{+2} ions from wastewater.

One of the challenging issues related to mercury adsorption on functionalized mesoporous materials is to achieve the total accessibility of the SH binding sites incorporated into the framework. Until now, new approaches have been focused on the design of well-ordered mesoporous materials with high sulfur content and large pore diameter, to assure Hg/S ratios ~ 1. Unfortunately, most of the studies have not reached this value due to channels blocking or to the fact that most of the functional groups are embedded into the silica walls.[34]

Here, we report the use of the novel thiol-ethylene bridged PMO material as a selective and regenerable mercury adsorbent. The material has the highest Hg^{2+} adsorption capacity obtained on well-ordered mesoporous materials currently known. Furthermore, regeneration and selectivity experiments show its enormous advantages as unique adsorbent material. Strikingly, the thiol groups uniformly present on the pore walls are able to induce the formation of Hg-S-Hg chains arranged in a cinnabar-like crystal structure.

2. Experimental section

2.1. Materials

Grubbs catalyst 1st generation ($RuP_2Cl_2H_{72}C_{43}$, 97%), 2,2-dimethoxy-2-phenylacethophenone (DMPA, 99%), thioacetic acid (CH_3COSH, 96%), Pluronic P123 surfactant (P123 triblock copolymer $EO_{20}PO_{70}EO_{20}$), propylamine ($CH3CH_2CH_2NH_2$, 98%), diisopropylethylamine (DIPEA, 99%) and sodium hydroxide (NaOH) were purchased from Aldrich. Propylamine was distilled on sodium hydroxide under inert

atmosphere. Vinyltriethoxysilane (VTES, 98%) and 1,2-bis(triethoxysilyl)ethane (BTEE, 97%) were supplied by abcr. Hydrochloric acid (HCl, 37%), nitric acid (HNO_3, 65%) and potassium chloride (KCl, 99.5%) were obtained from Carl Roth. Mercury nitrate solution ($Hg(NO_3)_2 \bullet H_2O$, 0.05 mol/l), was bought from ChemLab. $Pb(NO_3)_2$, $Zn(NO_3)_2$, $Cu(NO_3)_2$ and $Cd(NO_3)_2$ 1000 ppm standard solutions were purchased from ChemLab. Cysteine hydrochloride monohydrate (99%) was purchased from Roth. 5,5'-dithiobis-(2-nitrobenzoic acid) (DTNB, 98%) was purchased from TCI and methanol was purchased from Fisher Scientific. All chemicals were used without further purification.

2.2. Synthesis of thiol-functionalized ethylene-bridged PMOs (nSH-PMO)

Thiol-functionalized ethylene-bridged PMOs were prepared via self-assembly assisted co-condensation of the homemade thiol-ethylene bridged alkoxysilane, TBTEE (1-thiol-1,2-bis(triethoxysilyl)ethane), and one conventional silica source, BTEE (1,2-bis(triethoxysilyl)ethane) (Scheme 1). For a typical synthesis, P123 (0.42 g) and KCl (2.68 g) were dissolved in a solution of water (14.76 ml) and HCl (2.1 ml, 37 %). After stirring this solution overnight at 45 ºC, a mixture of silane precursors (TBTEE and BTEE) was added dropwise under vigorous stirring. The molar ratio of the reaction mixture was 1.0 Si:6.9 KCl:158.5 H_2O:4.9 HCl:0.013 P123. The resulting mixture was stirred at 45ºC for 24 h after which it was aged at 100 ºC for 24 h under static conditions. A white powder was recovered by filtration and thoroughly washed with H_2O. P123 template was removed from the products by three subsequent solvent extractions in a solution of 4 ml HCl (37%) in 150 ml ethanol at 80 ºC for 12h. Finally, the solid was filtered, washed with ethanol and dried under vacuum at 120 ºC. Samples with different thiol content are referred to as *n*SH-PMO where *n* (n=100, 75, 50 and 25) is the molar percent of TBTEE in the initial silane precursor mixture.

2.3. Ellman`s procedure

To determine the thiol content, nSH-PMO materials were analyzed by Ellman's reagent. [37] Typically, 50 mg of PMO was added to a solution of 0.1 g Ellman's reagent (5,5'-dithiobis-(2-nitrobenzoic acid, DNTB) and 500 µl of N,N-diisopropylethylamine (DIPEA) in approximately 50 ml of methanol. The mixture was mechanically shaken for 24 h. The PMO was then filtered through a membrane filter and washed with methanol. The absorbance of the solutions was measured at 409 nm, which is the maximum wavelength of absorbance for 2-nitro-5-thiobenzoate anion (TNB^{2-}) (Scheme 2).

2.4. Mercury adsorption experiments

The Hg^{2+} adsorption capacities for thiol-functionalized ethylene-bridged periodic mesoporous organosilicas were measured using a batch adsorption process. Typically, 50 mg of the PMO adsorbent was added to 50 ml of $Hg(NO_3)_2$ aqueous solution and the suspension was mechanically shaken at room temperature for 24 h. The mercury concentration of the solution (mercury concentrations of 2500, 1800, 1150 and 600 ppm) was such that the molar ratio of Hg^{2+} to the total sulfur content of the PMO was 3:1. The pH of the mercury solution was adjusted to 2.0 with HNO_3 prior to the adsorption to prevent precipitation of the metal ions during the adsorption experiments. After adsorption, the mixture was filtered. The mercury concentrations in the filtrate and in the initial solution were determined by AAS. Each adsorption experiment was performed in triplicate. The standard deviations for the AAS measurements are (in mg/g) 1.7 (100SH-PMO), 1.7 (75SH-PMO), 8.0 (50SH-PMO) and 1.2 (25SH-PMO).

2.5. Desorption and Regeneration experiments

Adsorption processes were performed according to the procedure described above but, in this particular case, with a molar ratio of Hg^{2+} in solution to the total sulfur content of the PMO of 1.2:1. After adsorption, the PMO adsorbent was recovered by filtration and washed repeatedly with distilled water. Then, the solid was added to 40 mL of a 1M HCl solution containing 2g of thiourea to desorb the mercury. The mixture was stirred at room temperature for 2 h and subsequently filtered. The solid was washed twice by stirring in distilled water for 30 min followed by filtration to complete the adsorption-desorption cycle. Finally, the PMO adsorbent was dried under vacuum at 120 ºC. To study the regeneration, three consecutive adsorption-desorption cycles were performed. Each experiment was performed in triplicate. Standard deviations (in mg/g) ranged from 5-18 (50SH-PMO), 3-30 (75SH-PMO) and 1-77 (100SH PMO).

2.6. Selective adsorption experiments

The heavy metal ions adsorption capacities for thiol-functionalized ethylene-bridged PMOs were also measured with a batch adsorption process. Typically, 50 mg of the adsorbent was added to 50 ml of a binary aqueous solution containing $Hg(NO_3)_2$ and either $Zn(NO_3)_2$, $Pb(NO_3)_2$ $Cu(NO_3)_2$ or $Cd(NO_3)_2$, which was adjusted to pH 2. In this case, the molar ratio of the sulfur content of the PMO to the Hg^{+2} and the competitive heavy metal (M^{+2}) in solution was 1 S: 1.2 Hg^{2+}: 1.2 M^{+2}. The M^{2+} concentration of the binary solutions was 1000, 720, 460 and 240 ppm. The mixture was mechanically shaken at room temperature for 24 h and filtered. The metal concentrations (Hg^{+2} and M^{+2}) in the filtrate and in the initial solutions were measured by AAS. Each experiment was performed in duplicate. Standard deviations (in mg/g) ranged from 0-12 for Hg, 0-6 for Zn, 1-22 for Pb, 1-6 for Cd and 1-8 for Cu.

2.7. Characterization

XRD measurements were performed on an ARL X´TRA powder diffractometer using CuKα radiation (45 kV and 44 mA). Nitrogen adsorption-desorption isotherms were determined on a Micromeritics TriStar 3000 analyzer at -196 ºC. Prior to measurement, the samples were outgassed overnight at 120ºC. DRIFT spectra were collected on a Thermo FTIR spectrometer. FT-Raman spectra were obtained using a Renishaw Raman Spectrometer. Elemental analysis (CHNS) was performed on a Thermo Flash 2000 elemental analyzer. XPS spectra were recorded with a SPECS Phoibos HAS 3500 150 MCD. Accurate binding energies (BE) were determined with respect to the position of the C 1s peak at 284.8 eV. Atomic absorption spectroscopy (AAS) was performed with a Varian SpectraAA 220FS. High Angle Annular Dark Field Scanning Transmission Electron Microscopy (HAADF-STEM) imaging and Energy-dispersive X-ray (EDX) spectroscopy experiments were performed on a FEI Titan "cubed" microscope, operated at 300 kV acceleration voltage and equipped with a large solid-angle "Super-X" EDX detector.

3. Results and discussion

3.1. Characterization of SH-ethane Periodic Mesoporous Organosilicas Adsorbents.

The X-ray diffraction patterns indicate that all thiol-functionalized ethylene-bridged PMO prepared at different molar ratios of TBTEE and BTEE precursors in the initial synthesis mixture possessed a well-ordered two-dimensional hexagonal structure (Fig. S1). The template-extracted samples exhibited three characteristic diffraction peaks in the low-angle region corresponding to (100), (110) and (200) reflections of a hexagonal *p6mm* symmetry. A progressive decrease in peak intensity was parallel to the increase of thiol groups incorporated in the ethane PMO matrix. Similarly, a slight shift

of these peaks towards higher 2θ values was observed as the TBTEE amount increased in the reaction mixture. This gradual shrinkage of the unit cell dimension from 11.7 to 10.5 nm for 25SH-PMO and 100SH-PMO, respectively, can be attributed to the structural contraction as a consequence of the formation of oxidation products (disulfide -S-S- bridges) between two adjacent SH groups (vide infra).

The nitrogen sorption measurements showed type-IV isotherms [38] (Fig. S2) with a sharp capillary condensation step in the relative pressure range of 0.5 – 0.7, characteristic of materials with well-ordered mesostructures. An H1-type hysteresis loop was observed in the isotherms, suggesting uniform cylindrical mesopores. These results further confirmed that the thiol-functionalized ethylene-bridged PMO with high amount of thiol groups had a high degree of structural ordering and a narrow pore size distribution. On the basis of the nitrogen adsorption isotherms, these nSH-PMO materials possessed high surface areas (569 – 696 m^2/g), large pore volumes (0.6 – 0.7 cm^3/g) and large pore diameters (4.7 – 5.5 nm) (Table 1). As the thiol content increased, a shift of the capillary condensation step to lower pressure values was observed, indicating the decrease in pore size. These results were consistent with the decrease of unit cell lattice calculated from XRD data.

DRIFT spectra of nSH-PMO materials are shown in Fig. S3. The presence of both organic bridging moieties (-CH_2-CH(SH)- and -CH_2-CH_2-) was confirmed by a group of bands in the range 2870-2918 cm^{-1}, which can be attributed to the stretching modes of CH_2 ($\upsilon_{s,as}$) and CH ($\upsilon_{s,as}$) groups.[34] A weak adsorption band around 2560 cm^{-1} corresponded to S-H stretching of thiol groups.

FT-Raman spectra further corroborated the presence of the thiol-functionality in the nSH-PMO samples, as shown in Fig. 1. An intense peak at 2560 cm^{-1}, consistent with the S-H stretching mode of thiol groups,[39] was observed in all thiol-functionalized ethylene-bridged PMO samples, clearly evidencing the successful co-condensation between TBTEE and BTEE. The intensity of this vibration is directly related to the –SH content present in each sample. Additionally, FT-Raman spectra featured a band associated with the vibration modes of S-S moieties around 520 cm^{-1}.[40-42] Disulfides are formed as a consequence of the air oxidation of the thiol groups.

To quantify both sulfur functional groups (-SH and –S-S- functionalities), nSH-PMO materials were analyzed using elemental analysis and Ellman's reagent (Table 2).[37, 43] The ratios of SH and SS groups determined by Raman intensities were consistent with those determined by elemental analysis and Elmman's reagent titration for both 25SH-PMO and 50SH-PMO. Taking into consideration the limitations of the Elmman's reagent for the quantification of closely located –SH groups, the –SH and –S-S- contents for 100SH-PMO and 75SH-PMO were calculated by the peak intensities of the respective Raman peaks, using the conversion factors obtained for the 25SH-PMO and 50SH-PMO samples.

3.2. Heavy metal uptake.

3.2.1. Hg adsorption study

The accessibility and capacity of –SH groups embedded into the porous walls of nSH-PMO to remove Hg^{2+} from aqueous metal solutions were investigated (see

Experimental Section for details). The maximum Hg^{2+} adsorption capacities are listed in Table 3.

All nSH-PMO samples were very efficient mercury adsorbents. Their adsorption capacity increased almost linearly with their sulfur content. The maximum mercury adsorption capacity reached 1183 mg/g for 100SH-PMO. This value is particularly high, compared to values reported in literature for other thiol-modified mesoporous silicas[8, 44-50] or organosilicas (PMOs).[29, 33, 34] Aguado *et al*.[51] reported a maximum adsorption capacity of 820 mg/g for a SH-functionalized SBA-15 and Wu *et al*.[32] reported a value of 464 mg/g for a SH-functionalized PMO. Likewise, in comparison to PMOs containing disulfide bridging groups, 100SH-PMO exhibited higher adsorption efficiency than that observed for disulfide-bridged PMO with high disulfide loading.[27, 28] Although, tetrasulfide-bridged mesoporous organosilicas can reach adsorption capacities of up to 2710 mg/g, it is worthy to mention the less ordered arrangement and non-uniform mesoporosity characteristics of this type of materials.[25] The calculated Hg/S ratios for the nSH-PMO samples were in the range 1.06 – 1.54 but in all cases higher than 1. These values suggest that all thiols in each adsorbent were accessible for the mercury ions. As the value was higher than 1, some sulfur moieties adsorbed more than one mercury ion. This is explained by the presence of disulfide species which can coordinate more than one mercury atom. This higher uptake is attributed to the stereo-coordination chemistry of S with Hg^{2+}.[25]

3.2.2. Selectivity study

The binding ability of nSH-PMO to capture other heavy metal ions in the presence of Hg^{2+} was studied using binary solutions containing equal concentrations of Hg^{2+} and M^{2+} (M^{2+} = Zn^{2+}, Pb^{2+} , Cu^{2+} or Cd^{+2}). Table 4 summarizes the adsorption capacity for Hg^{2+} and the above mentioned heavy metal ions by nSH-PMO samples. All

thiol-functionalized ethylene-bridged PMOs showed very high affinity for Hg^{2+} compared to other competitive heavy metals ions. The adsorption capacity of Hg^{2+} in the presence of Zn^{2+} and Cu^{2+} was comparable to the monocationic solution. Although the Hg^{2+} uptake decreased in the presence of those heavy metals with higher ionic radii such as Pb^{2+} and Cd^{2+}, it was still very high. The maximum adsorption capacities for Zn^{2+}, Pb^{2+}, Cu^{2+} and Cd^{2+} were not higher than 15, 90, 63 and 21mg/g, respectively, indicating the low binding affinity of these metal ions towards thiol and disulfide groups embedded into the porous framework. This lack of affinity of sulfur ligands to bind with other d^{10} metal ions (such as Zn^{2+}, Pb^{2+}, Cu^{2+} or Cd^{2+}) was observed for the first time by Pinnavaia *et al.*[52] for thiol-functionalized nanoporous silicas. They tentatively explained this effect by the thermodynamic inability of these metal ions to coordinate within the confined spaces of pore channels. Therefore, the uniform porosity of the nanostructured adsorbents is very important for their selective adsorption behavior.

3.2.3. Regeneration study

In order to investigate the reusability of the adsorbents, three consecutive adsorption-desorption cycles were performed. Fig. 2 shows the Hg^{2+} adsorption capacities of 100SH-PMO, 75SH-PMO and 50SH-PMO materials for three consecutive adsorption cycles. As can be observed, the adsorption capacity of 100SH-PMO decreases from 999 to 692 mg/g between the first and second cycle. A possible explanation can be due to the non-complete desorption of Hg ions from pores after treatment with acidic thiourea solution. 80% of the Hg^{2+} adsorbed in the first cycle was recovered in the thiourea solution. However, these values confirmed that thiol-functionalized ethylene-bridged PMO can retain more than 70% of its original adsorption capacity. As comparison, two good thioether-bridged PMO adsorbents with

Hg^{2+} adsorption capacities of 1500 and 627 mg/g retained less than 38% of their original capacity after the first cycle.[25, 26] Subsequent cycles were not reported. A vulcanized ethenylene bridged PMO[31] kept a constant Hg^{2+} capacity during three consecutive cycles but with values around 200 mg/g. To the best of our knowledge, there are no other reports that discuss the regeneration and reuse during consecutive cycles of such sulfur-containing PMO adsorbents. Therefore, 100SH-PMO can be considered as the first thiol mesoporous organosilica material with a mercury adsorption capacity of 767 mg/g in the third adsorption-desorption cycle.

The structural integrity of the materials after each consecutive adsorption cycle was investigated by XRD and nitrogen sorption. All nSH-PMO materials after each desorption step retained type-IV isotherms (Fig. S4-S6). The N_2 sorption isotherms showed a slight decrease in BET surface area after the first and second cycle (Table S1). This tendency was more pronounced with increasing the sulfur content of the PMO. However, after a first decrease in surface area, it stabilized for the consecutive runs. This decrease can be explained by the presence of residual adsorbed mercury or thiourea species on the PMO surface, as up to 20% of Hg^{2+} species remained on the regenerated materials in 100SH-PMO. This is also in accordance with the decrease in adsorption capacity observed in the second and third adsorption-desorption cycle.

Likewise, the XRD patterns showed that all samples preserved the hexagonal ordered mesostructured of the parent materials (Fig. S7). A reduction of the unit cell dimension was observed after the first cycle but subsequently it remained constant. This is in accordance with a shift of the capillary condensation step towards lower relative pressures in the nitrogen sorption isotherms. This is due to structural contraction, which occurs during the treatment in acidic solutions. These data show that after three subsequent treatments in acid mercury solutions, as well as in the acidified thiourea

solutions, the PMO materials retained their mesoporous structure. The high hydrothermal stability of PMO materials compared to their silica counterparts is a clear advantage for their use as robust adsorbents.[53] Overall, it is clear that these materials perform well in subsequent adsorption cycles.

3.3. Hg-S binding studies after Hg uptake

The Hg-S binding on nSH-PMO samples was studied by XPS, Raman and microscopy.

3.3.1. X-Ray photoelectron spectroscopy

The XPS spectra for the nSH-PMO and Hg-loaded nSH-PMO samples are shown in Fig. S8. The binding energies of Si2p, C1s and O1s were not influenced by the mercury adsorption. However, a new peak at 101 eV corresponding to Hg4f appeared after the mercury uptake on 100SH-PMO material. The high resolution S2p spectrum showed a slight shift of the S2p peak to lower binding energies likely due to the newly-formed Hg-S bond (Fig. 3 left).[31, 54-56] Since the position of the Hg4f signal overlapped with that of Si2p, the signal of Hg4d orbital was collected to evaluate the adsorption of Hg on 100SH-PMO (Fig. 3 right). After mercury adsorption, the Hg 4d XPS spectrum showed two intense signals at 362 and 381 eV assigned to $Hg4d_{5/2}$ and $Hg4d_{3/2}$, respectively. This result confirmed the absence of metallic Hg on the PMO surface.[57, 58]

3.3.2. Raman spectroscopy

The Raman spectra of 100SH-PMO and Hg-loaded 100SH-PMO are shown in Fig. 4. After mercury adsorption, the characteristic S-H stretching mode at 2560 cm^{-1} disappeared completely, indicating that all thiol-groups within the PMO framework were accessible to Hg^{2+} ions and were involved in complexation to mercury. Moreover,

two intense vibration bands appeared at 317 and 275 cm^{-1} assigned to the Hg-S stretching mode. The presence of a sharp band at 1044 cm^{-1} was associated to the free (uncoordinated) nitrate ion. The relative intensity of this band increased with increasing Hg loading (Fig. S9). So, both stretching bands (-NO_3 and Hg-S) become more intense in the higher sulfur containing samples. Additionally, Hg-loaded 100SH-PMO showed an intense vibration band at 166 cm^{-1}, which can be tentatively assigned to the presence of Hg_2^{2+}.[59, 60] These results are consistent with those reported by Pinnavaia et al.[41] in thiol-functionalized mesostructured silica. These authors assigned a cationic binding mode for Hg^{+2} ions bound to thiol ligands at high mercury loading (Hg/S 1.0-1.3). These results were confirmed by the presence of free nitrate ions in the Raman spectrum along with atomic pair distribution function (PDF) analysis of synchrotron X-ray power diffraction results. They proposed the formation of a polymeric $Hg(SR)^+$ species at high mercury loadings in which the mercury centers adopt a linear 2-fold coordination to bridging thiolate ligands.

3.3.3. Scanning transmission electron microscopy

Local scale investigation of Hg adsorption into the nSH-PMO material was performed by HAADF-STEM and EDX measurements. Electron microscopy techniques have proven to be extremely effective in characterizing mesoporous (organo)silicas and metallic, oxide or semiconductor materials embedded within these materials.[61-64] In Fig. 5, Z-contrast HAADF-STEM images of the 25SH-PMO material after Hg uptake are displayed. Elongated bright contrast nanoparticles, corresponding to a Hg-rich material, were aligned along the PMO pores (examples indicated by arrows in Fig. 5a). The pores of the PMO material were clearly organized into a hexagonal arrangement (Fig. 5b). When viewing the material along the pore direction, it can be seen that the Hg-rich nanoparticles were confined to single pores of the PMO structure (example

indicated by an arrow in Fig. 5b). In order to determine whether the Hg-containing particles were crystalline or not, high resolution HAADF-STEM images of the nanoparticles in 25SH-PMO (Fig. 5c) and 100SH-PMO (Fig. S10) were acquired. The nanoparticles were clearly crystalline and, using the reflections in the Fourier transform pattern of the high resolution image (Fig. 5d), they could be identified as cinnabar phase HgS. This conclusion was further confirmed by energy-dispersive X-ray (EDX) mapping in Fig. 6. The bright-contrast particles were both mercury and sulfur-rich; the oxygen and silicon signals arose from the PMO framework.

a) A 25SH-PMO crystal viewed perpendicular to the pore direction. The bright contrast features are likely Hg-containing material. b) 25SH-PMO crystal viewed along the pore direction. The bright-contrast Hg-containing material is clearly confined to single pores. c) High resolution image of HgS particles in the 25SH-PMO sample together with the d) corresponding FT pattern evidencing the cinnabar phase of the particles.

The formation of mercury thiolate nanocrystals into the pores of functionalized SH-based PMOs was evidenced by N_2 adsorption-desorption measurements (Fig. 7). As can be observed for Hg-loaded 25SH-PMO, the nitrogen physisorption isotherm exhibited a characteristic two-step desorption.[65, 66] The first one at high relative pressure corresponds to the equilibrium desorption in open mesopores, while the second one at low relative pressure is related to cavitation of condensed nitrogen in the blocked mesopores. Likewise, the surface area was decreased from 696 m^2/g to 480 m^2g^{-1} after Hg uptake. This effect of pore blockage was gradually increasing on those samples containing higher values of sulfur in their composition (Fig. S11-S13). For instance, Hg-loaded 100SH-PMO showed a surface area not higher than 40 m^2/g (Table S2).

4. Conclusions

A thiol-ethylene bridged Periodic Mesoporous Organosilica, with controllable thiol loading, was synthesized directly from the corresponding home-made 1-thiol-1,2-bis(triethoxysilyl)ethane. This hexagonally ordered mesporous material contains up to 4.28 mmol S per gram, present as a combination of thiol groups and disulfide bridges. 1 gram thiol-ethylene PMO adsorbs up to 1183 mg Hg^{2+} from aqueous solution, and is very selective for Hg, also in the presence of competing heavy metals ions. The materials can be regenerated and reused several times. EDX mapping shows the even distribution of the S-containing groups throughout the material. HAADF-STEM measurements reveal the presence of thiolate nanocrystals in the pores of the PMO after mercury sorption.

Acknowledgment

D.E. thanks the F.W.O. Flanders (Fund Scientific Research) for a postdoctoral grant (3E10813W). J.O. acknowledges also F.W.O. Flanders, research project G006813N, and the research Board of Ghent University, UGent GOA (Concerted Research Actions) (grant 01G00710) for financial support. F. J. R.-S. acknowledges funding of this research by the Spanish Ministry of Economy and Competitiveness (Project MAT2013-44463-R), Andalusian Regional Government (FQM-346 group), and Feder Funds. The Titan microscope used for this investigation was partially funded by the Hercules foundation of the Flemish government. This work was supported by the Belgian IAP-PAI network.

References

[1] A. Carocci, N. Rovito, M.S. Sinicropi, G. Genchi, Mercury Toxicity and Neurodegenerative Effects, in: D.M. Whitacre (Ed.) Reviews of Environmental Contamination and Toxicology, Vol 229, 2014, pp. 1-18.
[2] S.V.S. Rana, Perspectives in Endocrine Toxicity of Heavy Metals-A Review, Biological Trace Element Research, 160 (2014) 1-14.
[3] M. Hasan, Y. Selim, K. Mohamed, Removal of chromium from aqueous waste solution using liquid emulsion membrane, Journal of hazardous materials, 168 (2009) 1537-1541.
[4] K.S.K. Reddy, A. Al Shoaibi, C. Srinivasakannan, Elemental mercury adsorption on sulfur-impregnated porous carbon - A review, Environmental Technology, 35 (2014) 18-26.
[5] F.-H. Wang, W. Jiang, Y. Fang, C.-W. Cheng, Preparation of Fe3O4 magnetic porous microspheres (MPMs) and their application in treating mercury-containing wastewater from the polyvinyl chloride industry by calcium carbide method, Chemical engineering journal, 259 (2015) 827-836.
[6] P. Liu, C.J. Ptacek, D.W. Blowes, R.C. Landis, Mechanisms of mercury removal by biochars produced from different feedstocks determined using X-ray absorption spectroscopy, Journal of Hazardous Materials, 308 (2016) 233-242.
[7] R.G. Pearson, Hard and soft acids and bases, Journal of the American Chemical Society, 85 (1963) 3533-3539.
[8] X. Feng, G. Fryxell, L.-Q. Wang, A.Y. Kim, J. Liu, K. Kemner, Functionalized monolayers on ordered mesoporous supports, Science, 276 (1997) 923-926.
[9] S. Dai, M.C. Burleigh, Y. Shin, C.C. Morrow, C.E. Barnes, Z. Xue, Imprint coating: a novel synthesis of selective functionalized ordered mesoporous sorbents, Angewandte Chemie International Edition, 38 (1999) 1235-1239.
[10] L. Mercier, T.J. Pinnavaia, Access in mesoporous materials: advantages of a uniform pore structure in the design of a heavy metal ion adsorbent for environmental remediation, Advanced Materials, 9 (1997) 500-503.
[11] R. Rostamian, M. Najafi, A.A. Rafati, Synthesis and characterization of thiol-functionalized silica nano hollow sphere as a novel adsorbent for removal of poisonous heavy metal ions from water: Kinetics, isotherms and error analysis, Chemical engineering journal, 171 (2011) 1004-1011.
[12] A.M. Burke, J.P. Hanrahan, D.A. Healy, J.R. Sodeau, J.D. Holmes, M.A. Morris, Large pore bi-functionalised mesoporous silica for metal ion pollution treatment, Journal of Hazardous Materials, 164 (2009) 229-234.
[13] S.A. Idris, S.R. Harvey, L.T. Gibson, Selective extraction of mercury(II) from water samples using mercapto functionalised-MCM-41 and regeneration of the sorbent using microwave digestion, Journal of Hazardous Materials, 193 (2011) 171-176.
[14] F. Hoffmann, M. Cornelius, J. Morell, M. Fröba, Silica-based mesoporous organic–inorganic hybrid materials, Angewandte Chemie International Edition, 45 (2006) 3216-3251.
[15] T. Asefa, M.J. MacLachlan, N. Coombs, G.A. Ozin, Periodic mesoporous organosilicas with organic groups inside the channel walls, Nature, 402 (1999) 867-871.
[16] S. Inagaki, S. Guan, Y. Fukushima, T. Ohsuna, O. Terasaki, Novel mesoporous materials with a uniform distribution of organic groups and inorganic oxide in their frameworks, Journal of the American Chemical Society, 121 (1999) 9611-9614.
[17] B.J. Melde, B.T. Holland, C.F. Blanford, A. Stein, Mesoporous sieves with unified hybrid inorganic/organic frameworks, Chemistry of Materials, 11 (1999) 3302-3308.
[18] P. Van Der Voort, D. Esquivel, E. De Canck, F. Goethals, I. Van Driessche, F.J. Romero-Salguero, Periodic mesoporous organosilicas: from simple to complex bridges; a

comprehensive overview of functions, morphologies and applications, Chemical Society Reviews, 42 (2013) 3913-3955.
[19] P. Van Der Voort, C. Vercaemst, D. Schaubroeck, F. Verpoort, Ordered mesoporous materials at the beginning of the third millennium: new strategies to create hybrid and non-siliceous variants, Physical Chemistry Chemical Physics, 10 (2008) 347-360.
[20] N. Mizoshita, T. Tani, S. Inagaki, Syntheses, properties and applications of periodic mesoporous organosilicas prepared from bridged organosilane precursors, Chemical Society Reviews, 40 (2011) 789-800.
[21] D. Esquivel, P. Van Der Voort, F.J. Romero-Salguero, Designing advanced functional periodic mesoporous organosilicas for biomedical applications, AIMS Materials Science, 1 (2014) 70-86.
[22] O. Olkhovyk, M. Jaroniec, Periodic mesoporous organosilica with large heterocyclic bridging groups, Journal of the American Chemical Society, 127 (2005) 60-61.
[23] O. Olkhovyk, M. Jaroniec, Polymer-templated mesoporous organosilicas with two types of multifunctional organic groups, Industrial & engineering chemistry research, 46 (2007) 1745-1751.
[24] O. Olkhovyk, S. Pikus, M. Jaroniec, Bifunctional periodic mesoporous organosilica with large heterocyclic bridging groups and mercaptopropyl ligands, Journal of Materials Chemistry, 15 (2005) 1517-1519.
[25] L.X. Zhang, W.H. Zhang, J.L. Shi, Z. Hua, Y.S. Li, J. Yan, A new thioether functionalized organic-inorganic mesoporous composite as a highly selective and capacious Hg2+ adsorbent, Chemical Communications, (2003) 210-211.
[26] J. Liu, J. Yang, Q. Yang, G. Wang, Y. Li, Hydrothermally Stable Thioether-Bridged Mesoporous Materials with Void Defects in the Pore Walls, Advanced Functional Materials, 15 (2005) 1297-1302.
[27] N. Hao, L. Han, Y. Yang, H. Wang, P.A. Webley, D. Zhao, A metal-ion-assisted assembly approach to synthesize disulfide-bridged periodical mesoporous organosilicas with high sulfide contents and efficient adsorption, Applied Surface Science, 256 (2010) 5334-5342.
[28] P.-J. Chiu, S. Vetrivel, A.S. Chiang, H.-M. Kao, Synthesis and characterization of cubic periodic mesoporous organosilicas with a high loading of disulfide groups, New Journal of Chemistry, 35 (2011) 489-494.
[29] E. De Canck, L. Lapeire, J. De Clercq, F. Verpoort, P. Van Der Voort, New ultrastable mesoporous adsorbent for the removal of mercury ions, Langmuir, 26 (2010) 10076-10083.
[30] Y. Gao, E. De Canck, M. Leermakers, W. Baeyens, P. Van Der Voort, Synthesized mercaptopropyl nanoporous resins in DGT probes for determining dissolved mercury concentrations, Talanta, 87 (2011) 262-267.
[31] M.a.I. López, D. Esquivel, C. Jiménez-Sanchidrián, P. Van Der Voort, F.J. Romero-Salguero, Vulcanized Ethene-PMO: A New Strategy to Create Ultrastable Support Materials and Adsorbents, The Journal of Physical Chemistry C, 118 (2014) 17862-17869.
[32] H.-Y. Wu, C.-H. Liao, Y.-C. Pan, C.-L. Yeh, H.-M. Kao, Synthesis and characterization of cubic thiol-functionalized periodic mesoporous organosilicas as effective mercury ion adsorbents, Microporous and Mesoporous Materials, 119 (2009) 109-116.
[33] H.-Y. Wu, C.-T. Chen, I.-M. Hung, C.-H. Liao, S. Vetrivel, H.-M. Kao, Direct synthesis of cubic benzene-bridged mesoporous organosilica functionalized with mercaptopropyl groups as an effective adsorbent for mercury and silver ions, The Journal of Physical Chemistry C, 114 (2010) 7021-7029.
[34] Q. Yang, J. Liu, J. Yang, L. Zhang, Z. Feng, J. Zhang, C. Li, Acid catalyzed synthesis of ordered bifunctionalized mesoporous organosilicas with large pore, Microporous and mesoporous materials, 77 (2005) 257-264.
[35] D. Esquivel, O. van den Berg, F.J. Romero-Salguero, F. Du Prez, P. Van Der Voort, 100% thiol-functionalized ethylene PMOs prepared by “thiol acid–ene” chemistry, Chemical Communications, 49 (2013) 2344-2346.

[36] J. Gehring, D. Schleheck, B. Trepka, S. Polarz, Mesoporous organosilica nanoparticles containing superacid and click functionalities leading to cooperativity in biocidal coatings, ACS applied materials & interfaces, 7 (2014) 1021-1029.
[37] R.P. Hodgkins, A.E. Garcia-Bennett, P.A. Wright, Structure and morphology of propylthiol-functionalised mesoporous silicas templated by non-ionic triblock copolymers, Microporous and mesoporous materials, 79 (2005) 241-252.
[38] K.S. Sing, Reporting physisorption data for gas/solid systems with special reference to the determination of surface area and porosity (Recommendations 1984), Pure and applied chemistry, 57 (1985) 603-619.
[39] E. Cano-Serrano, J. Campos-Martin, J. Fierro, Sulfonic acid-functionalized silica through quantitative oxidation of thiol groups, Chemical Communications, (2003) 246-247.
[40] G.J. Kluth, C. Carraro, R. Maboudian, Direct observation of sulfur dimers in alkanethiol self-assembled monolayers on Au (111), Physical Review B, 59 (1999) R10449.
[41] S.J. Billinge, E.J. McKimmy, M. Shatnawi, H. Kim, V. Petkov, D. Wermeille, T.J. Pinnavaia, Mercury binding sites in thiol-functionalized mesostructured silica, Journal of the American Chemical Society, 127 (2005) 8492-8498.
[42] K. Wilson, A.F. Lee, D.J. Macquarrie, J.H. Clark, Structure and reactivity of sol–gel sulphonic acid silicas, Applied Catalysis A: General, 228 (2002) 127-133.
[43] J.P. Badyal, A.M. Cameron, N.R. Cameron, D.M. Coe, R. Cox, B.G. Davis, L.J. Oates, G. Oye, P.G. Steel, A simple method for the quantitative analysis of resin bound thiol groups, Tetrahedron Letters, 42 (2001) 8531-8533.
[44] A. Arencibia, J. Aguado, J.M. Arsuaga, Regeneration of thiol-functionalized mesostructured silica adsorbents of mercury, Applied Surface Science, 256 (2010) 5453-5457.
[45] M. Barczak, M. Oszust, K. Michalak, K. Gdula, S. Pasieczna-Patkowska, E. Zięba, A. Dąbrowski, Functionalized SBA-15 organosilicas as sorbents of mercury (II), cadmium (II) and copper (II), Glass Physics and Chemistry, 40 (2014) 41-48.
[46] A. Walcarius, C. Delacôte, Mercury (II) binding to thiol-functionalized mesoporous silicas: critical effect of pH and sorbent properties on capacity and selectivity, Analytica Chimica Acta, 547 (2005) 3-13.
[47] J.M. Arsuaga, J. Aguado, A. Arencibia, M.S. López-Gutiérrez, Aqueous mercury adsorption in a fixed bed column of thiol functionalized mesoporous silica, Adsorption, 20 (2014) 311-319.
[48] S. Ravi, M. Selvaraj, H. Park, H.-H. Chun, C.-S. Ha, Novel hierarchically dispersed mesoporous silica spheres: effective adsorbents for mercury from wastewater and a thermodynamic study, New Journal of Chemistry, 38 (2014) 3899-3906.
[49] T.M. Abdel-Fattah, S.M. Haggag, M.E. Mahmoud, Heavy metal ions extraction from aqueous media using nanoporous silica, Chemical Engineering Journal, 175 (2011) 117-123.
[50] C. Lesaint, F. Frébault, C. Delacôte, B. Lebeau, C. Marichal, A. Walcarius, J. Patarin, Synthesis and characterization of mesoporous silicas functionalized by thiol groups, and application as sorbents for mercury (II), Studies in Surface Science and Catalysis, 156 (2005) 925-932.
[51] J. Aguado, J.M. Arsuaga, A. Arencibia, Influence of synthesis conditions on mercury adsorption capacity of propylthiol functionalized SBA-15 obtained by co-condensation, Microporous and Mesoporous Materials, 109 (2008) 513-524.
[52] T. Pinnavaia, Selective adsorption of Hg 2+ by thiol-functionalized nanoporous silica, Chemical Communications, (1999) 69-70.
[53] R. Otero, D. Esquivel, M.A. Ulibarri, C. Jiménez-Sanchidrián, F.J. Romero-Salguero, J.M. Fernández, Adsorption of the herbicide S-Metolachlor on periodic mesoporous organosilicas, Chemical engineering journal, 228 (2013) 205-213.
[54] G. Yang, H. Han, C. Du, Z. Luo, Y. Wang, Facile synthesis of melamine-based porous polymer networks and their application for removal of aqueous mercury ions, Polymer, 51 (2010) 6193-6202.

[55] N.D. Hutson, B.C. Attwood, K.G. Scheckel, XAS and XPS characterization of mercury binding on brominated activated carbon, Environmental science & technology, 41 (2007) 1747-1752.
[56] J. Wang, B. Deng, X. Wang, J. Zheng, Adsorption of aqueous Hg (II) by sulfur-impregnated activated carbon, Environmental Engineering Science, 26 (2009) 1693-1699.
[57] C.D. Wagner, G. Muilenberg, Handbook of X-ray photoelectron spectroscopy, Perkin-Elmer, 1979.
[58] S. Jayabal, R. Sathiyamurthi, R. Ramaraj, Selective sensing of Hg 2+ ions by optical and colorimetric methods using gold nanorods embedded in a functionalized silicate sol–gel matrix, Journal of Materials Chemistry A, 2 (2014) 8918-8925.
[59] M.S. Wickleder, Hg2 (CH3SO3) 2: Synthese, Kristallstruktur, thermisches Verhalten und Schwingungsspektroskopie, Zeitschrift für anorganische und allgemeine Chemie, 628 (2002) 1848-1852.
[60] H. Stammreich, T.T. Sans, Hg-Hg stretching frequencies and bond lengths in mercurous compounds, Journal of Molecular Structure, 1 (1967) 55-60.
[61] S. Liu, P. Cool, O. Collart, P. Van Der Voort, E.F. Vansant, O.I. Lebedev, G. Van Tendeloo, M. Jiang, The influence of the alcohol concentration on the structural ordering of mesoporous silica: cosurfactant versus cosolvent, The Journal of Physical Chemistry B, 107 (2003) 10405-10411.
[62] L.H. Wee, M. Meledina, S. Turner, K. Custers, S. Kerkhofs, G. van Tendeloo, J. Martens, Hematite iron oxide nanorod patterning inside COK-12 mesochannels as an efficient visible light photocatalyst, Journal of Materials Chemistry A, 3 (2015) 19884-19891.
[63] F. Lin, X. Meng, E. Kukueva, T. Altantzis, M. Mertens, S. Bals, P. Cool, S. Van Doorslaer, Direct-synthesis method towards copper-containing periodic mesoporous organosilicas: detailed investigation of the copper distribution in the material, Dalton Transactions, 44 (2015) 9970-9979.
[64] L. Wee, M. Meledina, S. Turner, K. Custers, S. Kerkhofs, S. Sree, E. Gobechiya, C. Kirschhock, G. Van Tendeloo, J. Martens, Anatase TiO 2 nanoparticle coating on porous COK-12 platelets as highly active and reusable photocatalysts, RSC Advances, 6 (2016) 46678-46685.
[65] P. Van Der Voort, P. Ravikovitch, K. De Jong, M. Benjelloun, E. Van Bavel, A. Janssen, A. Neimark, B. Weckhuysen, E. Vansant, A new templated ordered structure with combined micro-and mesopores and internal silica nanocapsules, The Journal of Physical Chemistry B, 106 (2002) 5873-5877.
[66] P. Van Der Voort, P. Ravikovitch, K. De Jong, A. Neimark, A. Janssen, M. Benjelloun, E. Van Bavel, P. Cool, B. Weckhuysen, E. Vansant, Plugged hexagonal templated silica: a unique micro-and mesoporous composite material with internal silica nanocapsules, Chemical Communications, (2002) 1010-1011.

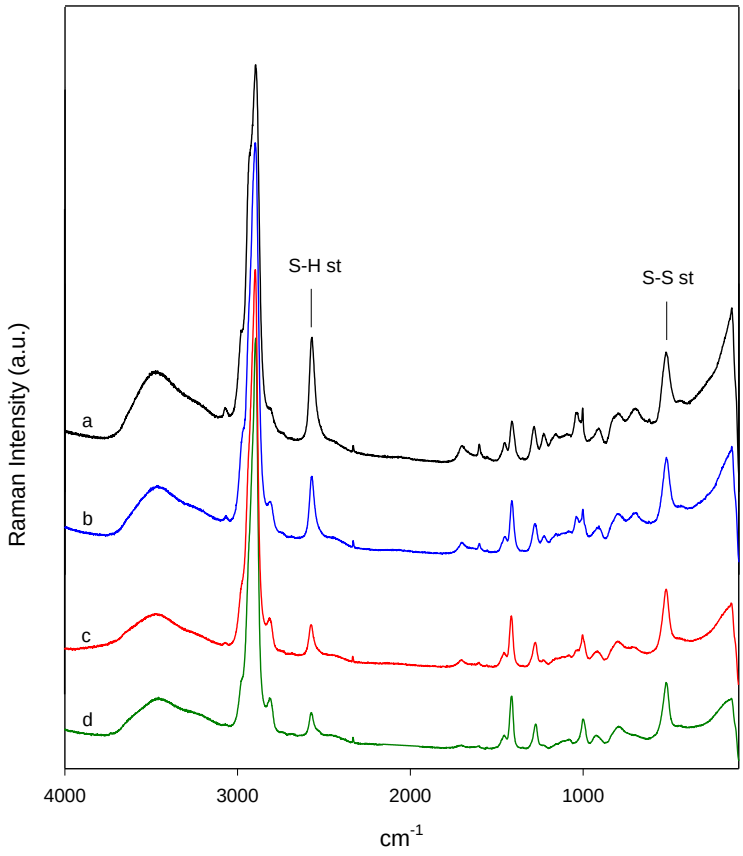

Fig. 1. FT-Raman spectra of thiol-functionalized ethylene-bridged PMOs. (a) 100SH-PMO, (b) 75SH-PMO, (c) 50SH-PMO and (d) 25SH-PMO.

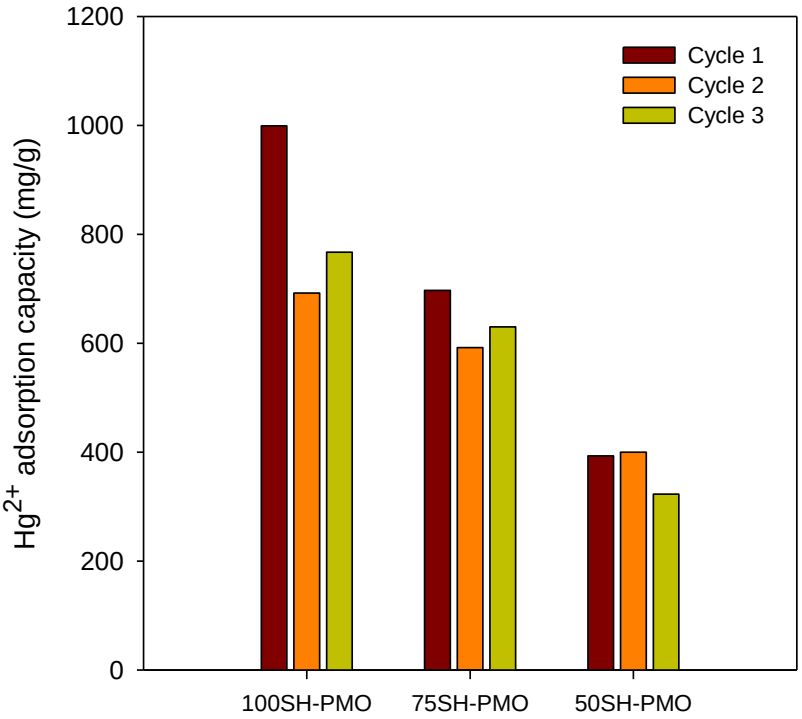

Fig. 2. Hg^{2+} adsorption capacities of nSH-PMO materials for three consecutive adsorption-desorption cycles.

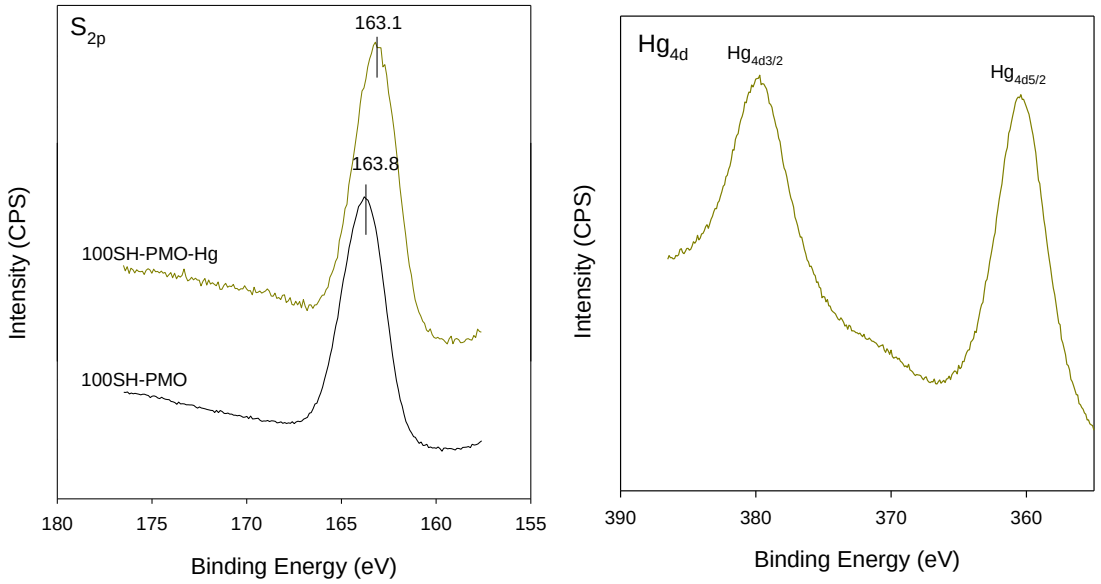

Fig. 3. X-ray photoelectron spectroscopy of 100SH-PMO and Hg-loaded 100SH-PMO samples. High resolution spectra of S2p (left) and Hg4d (right).

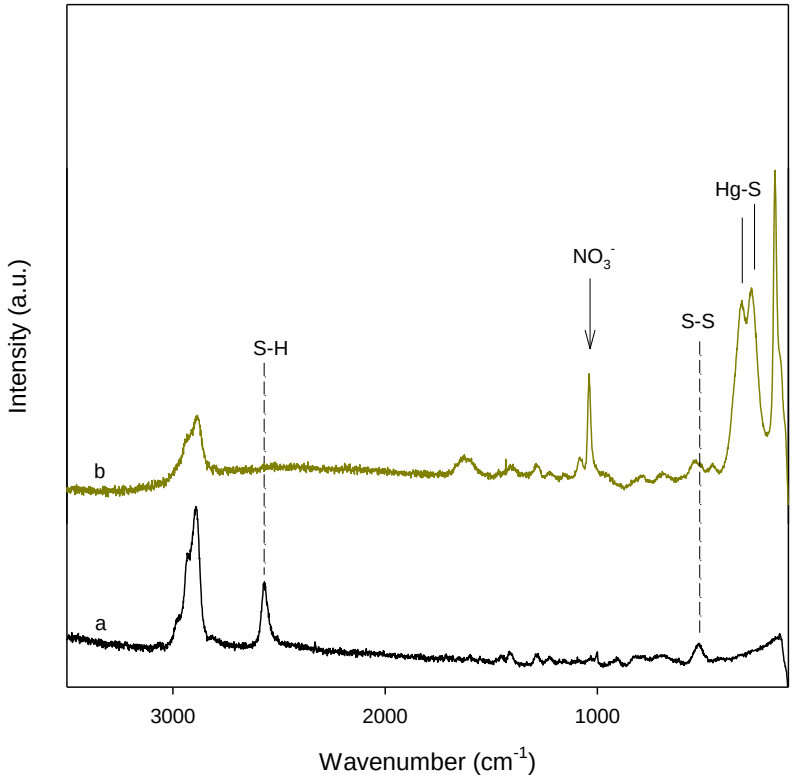

Fig. 4. FT-Raman spectra of 100SH-PMO (a) and Hg-loaded 100SH-PMO (b).

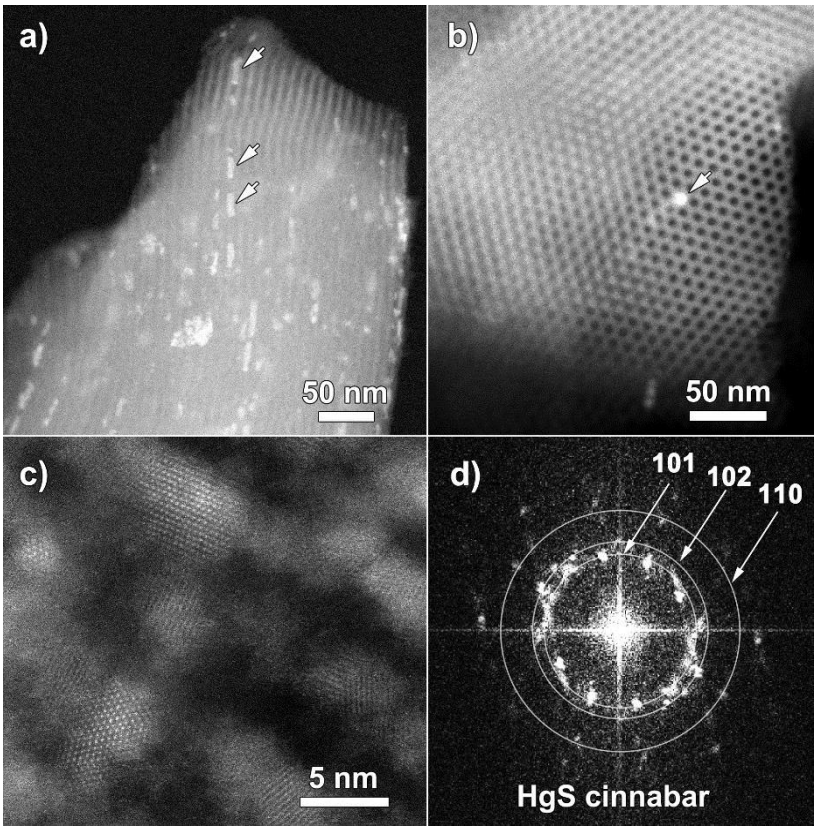

Fig. 5. HAADF-STEM images of the 25SH-PMO material after mercury uptake.

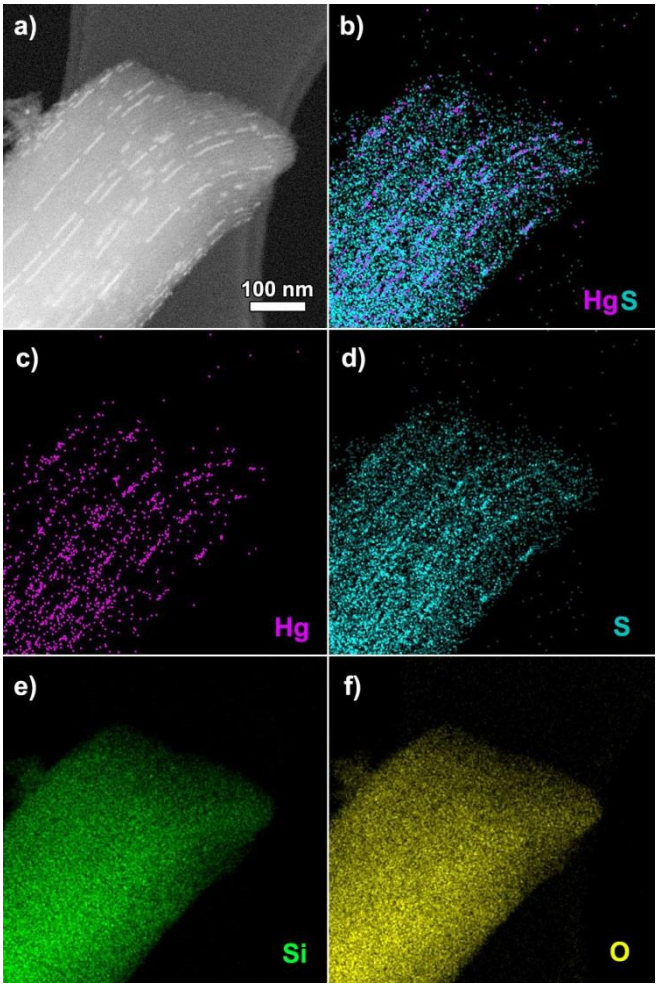

Fig. 6. a) HAADF-STEM image of a 25SH-PMO crystal after Hg uptake, viewed perpendicular to the pore direction, together with corresponding elemental EDX maps for b) Hg and S, c) Hg, d) S, e) Si and f) O.

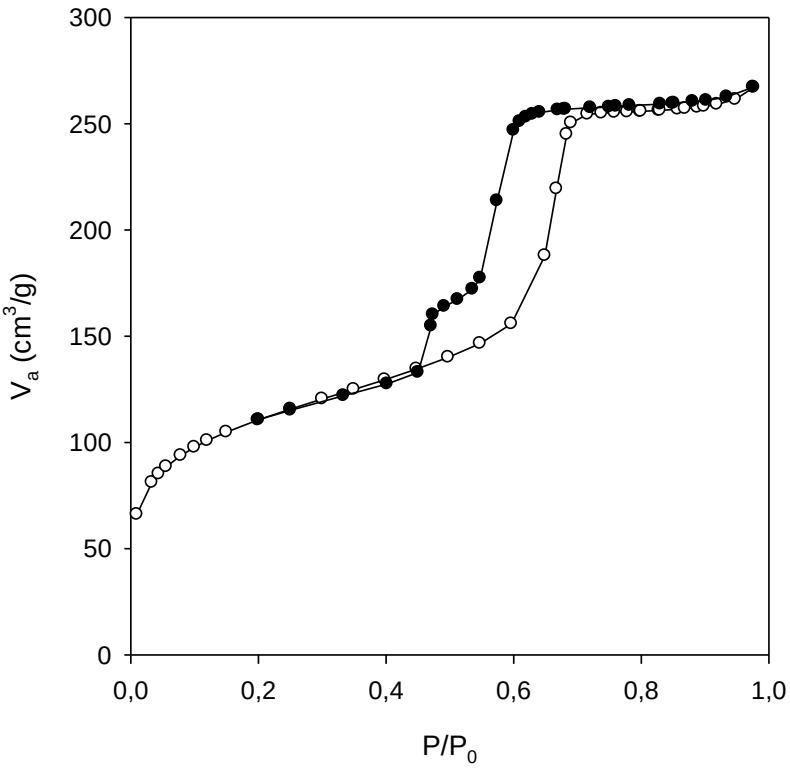

Fig. 7. N_2 adsorption-desorption isotherms of Hg-loaded 25SH-PMO.

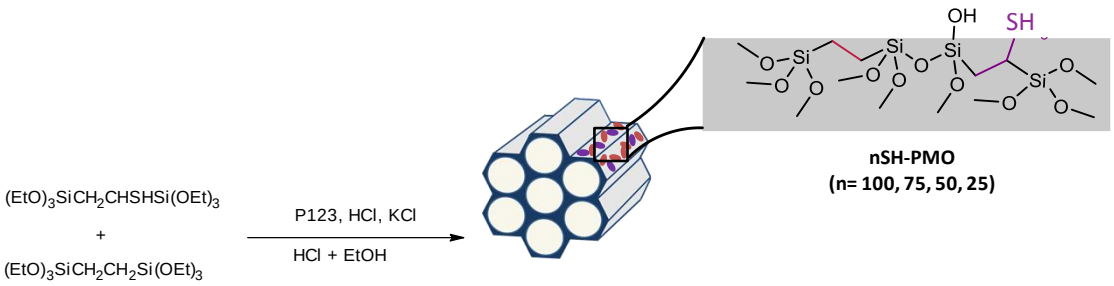

Scheme 1. Synthetic procedure of thiol-functionalized ethylene-bridged periodic mesoporous organosilicas (nSH-PMO).

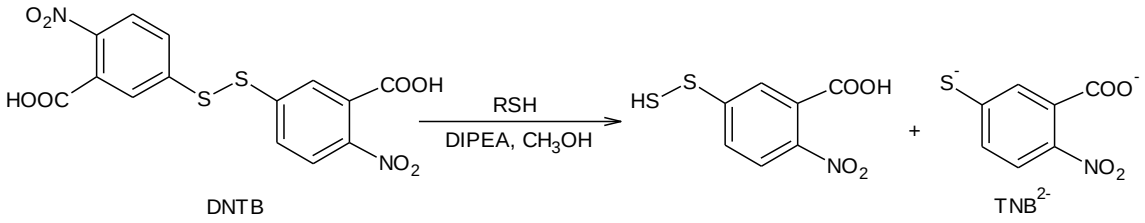

Scheme 2. Reaction of the Ellman reagent (DNTB) with a thiol group

Table 1. Structural and textural properties of nSH-PMO, where n represents the molar percent of thiol-precursor (TBTEE).

nSH-PMO samples	Molar ratio (TBTEE:BTEE)[a]	%C[b]	%S[b]	a_0[c] (nm)	S_{BET} (m^2/g)	V_p (cm^3/g)	d_p[d] (nm)	Wall thickness[e] (nm)
100SH-PMO	100:0	18.5	13.7	10.5	640	0.66	4.7	5.8
75SH-PMO	75:25	20.2	9.7	11.0	569	0.60	4.8	6.2
50SH-PMO	50:50	20.1	6.2	11.3	642	0.66	5.0	6.3
25SH-PMO	25:75	20.9	3.1	11.7	696	0.71	5.5	6.2

[a]TBTEE: 1-thiol-1,2-bis(triethoxysilyl)ethane; BTEE: 1,2-bis(triethoxysilyl)ethane. [b]Weight % determined by elemental analysis; [c]Lattice parameters a_0 were calculated based on the formula $a_0=2d_{100}/\sqrt{3}$; [d]Calculated from adsorption branch; [e]Calculated as the difference between a_0 and d_p.

Table 2. Sulfur content of the thiol-functionalized ethylene-bridged PMOs

Sample	S_{total} content (mmol/g)[a]	SH content (mmol/g)[b,c]	SS content (mmol/g)[d]
100SH-PMO	4.28	2.42[c]	1.86
75SH-PMO	3.03	1.34[c]	1.69
50SH-PMO	1.93	0.51[b]	1.42
25SH-PMO	0.96	0.24[b]	0.72

[a]Calculated from elemental analysis; [b]Determined by Elmman`s reagent; [c]Calculated from Raman spectroscopy (see text); [d]SS content was calculated as the difference between S_{total} content and SH content.

Table 3. Maximum mercury adsorption capacities for thiol-functionalized ethylene-bridged PMOs**.**

Sample	S_{total} (mmol/g)	Hg adsorption capacity (mg/g)	Hg/S_{total} ratio
100SH-PMO	4.28	1183 ± 2	1.38
75SH-PMO	3.03	833 ± 2	1.37
50SH-PMO	1.93	410 ± 8	1.06
25SH-PMO	0.96	297 ± 1	1.54

Table 4. Heavy metal ion adsorption capacities (mg/g) and removal efficiency (in brackets) for nSH-PMO materials in binary metallic solutions.

Sample	Hg-Zn		Hg-Pb		Hg-Cu		Hg-Cd	
	Hg^{2+}	Zn^{2+}	Hg^{2+}	Pb^{2+}	Hg^{2+}	Cu^{2+}	Hg^{2+}	Cd^{2+}
100SH-PMO	1036 (99.9%)	15 (1.6%)	677 (96.5%)	90 (9.8%)	994 (96.5%)	45 (4.3%)	673 (99.6%)	0 (0%)
75SH-PMO	802 (97.0%)	15 (2.1%)	502 (92.3%)	40 (5.7%)	695 (96.5%)	35 (4.8%)	535 (98.2%)	0 (0%)
50SH-PMO	532 (96.1%)	10 (2.1%)	319 (76.7%)	7 (1.5%)	439 (91.5%)	63 (12.9%)	321 (89.7%)	21 (4.8%)
25SH-PMO	245 (88.1%)	2 (0.9%)	138 (100%)	2 (0.9%)	172 (75.9%)	7 (3.1%)	134 (80.8%)	7 (3.2%)